Proceedings World Geothermal Congress 2020+1
Reykjavik, Iceland, April - October 2021

Evaluation of Casing Collapse Capacity in Ultra-High Temperature Geothermal Wells

Gaute Gruben, David Phillippe, Tèrence Coudert, Hieu Nguyen Hoang, Arve Bjørset, Sturla Sæther and Bård Nyhus

SINTEF Industry, Richard Birkelands veg 2B, No-7491, Trondheim, Norway

gaute.gruben@sintef.no

Keywords: Casing, Collapse, Ultra-High Temperature, Finite Element Analyses

ABSTRACT

A common cause of casing failure in geothermal wells are due to collapse caused by compressive hoop stress that occurs during heating of the well. In traditional design, the empirical formulas from API TR 5C3 are applied for determining the casing collapse capacity. However, the experimental data that constitute the foundation for the API formulas are limited in the range of axial stress and temperature. For high temperature geothermal wells, thermal expansion causes high axial compressive stresses, that might be outside the range of the API formulas. Another factor that is not included in the API formulas is the support from the surrounding cement. In this study, we use a combination of data from ultra-high temperature material testing and Finite Element Analyses to investigate the casing collapse capacity for load cases relevant for ultra-high temperature geothermal wells. The results from the Finite Element Analyses show that the collapse capacity increases for high levels of axial stress. This was observed for a wide range of material input data, diameter-wall thickness ratios and for un-supported and supported conditions.

1. INTRODUCTION

Geothermal wells operating at ultra-high temperatures (>450 °C) have a substantial potential for high energy output as compared to conventional geothermal wells that operate at 200-300 °C (Elders et al., 2014). However, there is a need for research and development before geothermal wells can operate in the ultra-high temperature regime, although substantial contributions have been made, most notably in the Iceland deep drilling project, see e.g. Friðleifsson et al. (2014). One of the challenges related to geothermal wells is collapse of the casing due to external pressure. This pressure occurs during heating of the well if the annular water is not vented into the rock formation or if the heating rate is too high (Kaldal et al., 2016). Clearly the risk of casing collapse increases with increased operating temperature. Additionally, compressive stresses build up in the casing during heating, and so an eventual collapse can occur at high compressive stresses. To the authors knowledge, no studies have been conducted on the casing collapse capacity at ultra-high temperatures and high axial stress. The present study aims to begin filling this gap of knowledge by performing numerical analyses of casing collapse in a wide range of axial stresses and with material data spanning from room temperature up to 500 °C.

2. FINITE ELEMENT MODELLING APPROACH

In order to validate the numerical modelling approach applied in this study, the experimental data from un-supported collapse tests with different axial stress given by Buchmiller et al. (2018), and supported collapse tests at zero axial stress provided by Hørte et al. (2020) is applied. Both studies provide collapse characteristics of a C110 steel casing with nominal outer diameter (OD) of 246.8 mm and a nominal wall thickness (t) of 13.5 mm. The dimensions of the C110 casing defines the geometry of the baseline numerical model applied in the present study. Details of the validation is to be presented in a future publication.

The numerical models are run with the commercial Finite Element (FE) software Abaqus/Standard (2020). In a collapse test, the stress, strain and displacement of the casing is symmetric at the longitudinal center of the specimen, thus a 4 OD (1 m) long segment with symmetry boundary condition (BC) at one end is modelled to represent a specimen with an effective length of 8 OD (2 m), see Figure 1(a). At the opposite side of the casing, all degrees-of-freedom (DOF) are fixed except the translateral DOF in the longitudinal direction of the casing (Z-direction in Figure 1(a)). The segment (with OD=246.8 mm and a wall thickness t =13.5 mm) is discretized by shell elements (Abaqus type S4R) with a characteristic element size equal to the wall thickness. Note that the pipe diameter as measured from the center of the shell element is OD$-t$=233.3 mm. The ovality in the FE model is set to 0.4 %.

The FE analyses are conducted in two steps; in the first step the axial loading is ramped up until the sought axial force, while in the second step the external pressure is ramped up under constant axial load. In order to capture the post-buckling equilibrium, an arc-length method is applied in the second load step, while a standard Newton-Raphson procedure is applied in the first step. The loading input parameters are the sought traction, T, in the axial direction at the end of the casing and a nominal external pressure value, P_0=100 MPa, on the outer casing. For each increment in the second step, the pressure loading is ramped up by a load proportionality factor (LPF), thus the effective pressure for each increment is $P = P_0 \cdot LPF$. Figure 1(a) illustrates the applied loads. The maximum loading (P_{max}) is reached at onset of bifurcation (collapse). After collapse, the LPF decreases since the external forces must be in equilibrium with the internal forces.

In the FE model of the supported casing, volume elements (Abaqus type C3D8R) are applied to discretize the support. Since the support is only subject to elastic deformations, a relatively coarse mesh was found sufficient; 3 elements are applied over the radial thickness, 40 elements are applied in the circumferential cross-section and 13 elements are used along the length, see Figure 1(b). The inner diameter of the support is 250 mm, and the thickness is 200 mm. Further, the support is given elastic properties similar to cement, i.e., a Young's modulus of 2.5 GPa and Poisson's ratio of 0.15. At the symmetry end, the support is fixed in the DOFs in the longitudinal direction, while all DOFs are fixed at the other end. The contact between the casing and the support is handled by a surface-to-surface contact accounting for finite sliding and with a coulomb friction coefficient of 0.01.

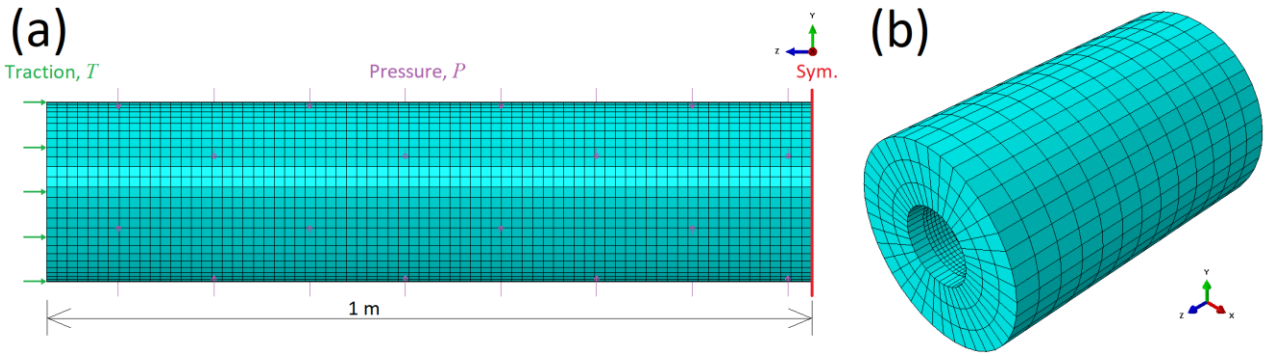

Figure 1: (a) FE mesh of casing specimen. The symmetry boundary condition and the loading are illustrated. (b) FE mesh of support outside the casing pipe.

An elasto-plastic material model is applied to describe the non-linear response of the material. The elastic properties are described by a Poisson ratio of 0.3 and Young's modulus found from tensile tests. The plasticity is described by the von Mises yield surface and the associated flow rule. Work hardening is modelled by Ludwik's power law which express the flow stress, σ_f^L, as

$$\sigma_f^L = A + B \cdot p^{n_L} \tag{1}$$

where A, B and n_L are parameters to be determined for each material and temperature.

3. PREDICTION OF COLLAPSE CAPACITY AT HIGH AXIAL STRESS

In this section we apply the FE modelling approach to estimate the collapse capacity at high axial stresses. High axial stresses are associated with high temperatures; thus, we apply material data generated from high temperature tests as well as data from room temperature tests.

3.1 Material data

Gruben et al. (2021) reported data from tensile tests on various casing materials conducted at 20 °C, 350 °C and 500 °C. Two of the investigated materials, where K55 and P110. Based on the raw data from the tests on these two materials, the parameters in Ludwik's power law were determined for 20 °C, 350 °C and 500 °C. The true stress-strain curves until onset of necking and the calibrated Ludwik power law curves are shown in Figure 2, and the calibrated Ludwik parameters are compiled in Table 1. The elastic properties of the materials are given by a Young's modulus found from the tensile tests, see Table 1, and an assumed Poisson's ratio of 0.3. Notably the Young's modulus values (E) given in Table 1 are close to the values at room temperature and at 350 °C in NZS 2403:2015 (2015), and a significant decrease in the Young's modulus is present when increasing the temperature from 350 °C to 500 °C.

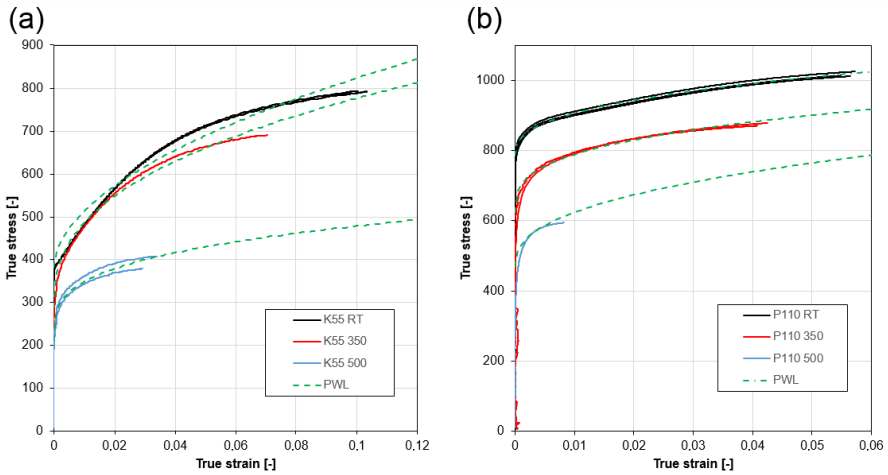

Figure 2: Experimental true stress vs true plastic strain curves and fitted Ludwik power law curves for (a) K55 and (b) P110 casing steels, at 20 °C, 350 °C and 500 °C

Table 1 Data from K55 and P110 casing materials (Gruben et al., 2021). Yield stress (R_{p02}), tensile stress (R_m), yield to tensile ratio, Youngs modulus (E) and calibrated Ludwik power law parameters (A, B and n_L)

Material	Temperature	R_{p02} (MPa)	R_m (MPa)	R_{p02}/R_m	E (GPa)	A (MPa)	B (MPa)	n_L
K55	20 °C	397	714	0.56	215	380	1473	0.52
	350 °C	374	643	0.58	177	288	1205	0.39
	500 °C	296	380	0.78	136	213	520	0.29
P110	20 °C	848	958	0.89	211	785	699	0.38
	350 °C	704	835	0.84	177	623	728	0.32
	500 °C	542	587	0.92	137	469	987	0.40

3.2 Collapse capacity for un-supported casing

The predicted collapse capacity for the K55 and P110 materials at 20 °C, 350 °C and 500 °C are calculated from FEA and API TR 5C3 (2019) for a range of axial stresses spanning from zero to $1.2R_{p02}$ (note that API TR 5C3 does not account for axial stress). Here the axial stress is defined as the axial force divided by the initial cross-section area of the casing, i.e. the nominal average axial stress. Further, the collapse pressure is given as a function of the normalized axial stress, i.e. for each material and temperature the axial stress is divided by the yield stress, R_{p02}, as given in Table 1. For each material/temperature combination, FEA is run with normalized axial stress of 0, 0.3, 0.6, 0.9, 1.0, 1.1 and 1.2. The results are shown in Figure 3. The K55 material have a collapse capacity spanning from ~28 MPa to ~48 MPa, while the P110 material have a collapse capacity spanning from ~44 MPa to ~73 MPa. By inspecting the values in Table 1 and Figure 3, there is a clear correlation between R_{p02} and the collapse capacity as estimated from FEA. Although there are differences in yield strength, work hardening and Young's modulus, the FEA predicts that the K55 material at 20 °C and the P110 material at 500 °C have nearly the same collapse capacity in the investigated span of axial stresses. Further, the FEA results for K55 at 20 °C and 350 °C indicate that a decrease in Young's modulus decreases the collapse capacity.

For all materials, the FEA collapse capacity increase when increasing the axial stress until approximately $0.5R_{p02}$ and then decreases when the axial stress is increased further until it reaches a minimum around $0.9 - 1.0R_{p02}$. Interestingly, the collapse capacity for all materials increase when the axial stress is further increased above R_{p02}. The increase in collapse capacity for high axial stresses could stem from the increased flow stress in the material, i.e. an effect similar to increasing the materials yield strength. The FE analyses generally predict a higher collapse capacity than API TR 5C3. However, the difference is largest at room temperature and decreases for 350 °C. At 500 °C the difference in collapse capacity predicted by FEA and API TR 5C3 is very small. This could be related to the reduction in Young's modulus that is included in the FEA, but not in API TR 5C3.

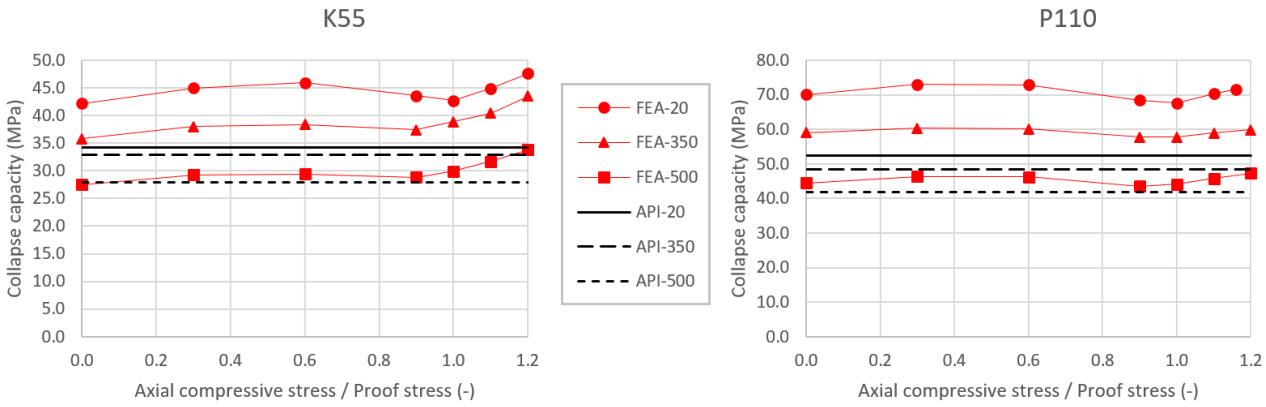

Figure 3: FEA and API predictions of collapse pressure for K55 and P110 materials at different temperatures and axial stresses.

3.3 Collapse capacity for supported casing

In this section we will focus on the K55 and the P110 materials at 500 °C as these temperatures are considered the most relevant for high axial loading situations. Since this type of buckling analyses can lead to a bifurcation point, where the model follows a non-physical equilibrium path, care was taken to ensure that all simulations had a realistic deformation mode after collapse (bifurcation), see Figure 4(a).

As can be seen from Figure 4(b), also the supported conditions predict an increase in collapse capacity when the axial loading is increased above $0.9R_{p02}$. In particular, the P110 material with the highest axial load ($1.2R_{p02}$) have a large increase in collapse pressure. Further, it is found that the supported conditions lead to a ~23% increase in collapse capacity for K55 and ~33% increase in collapse capacity for P110 (excluding the point at $1.2R_{p02}$).

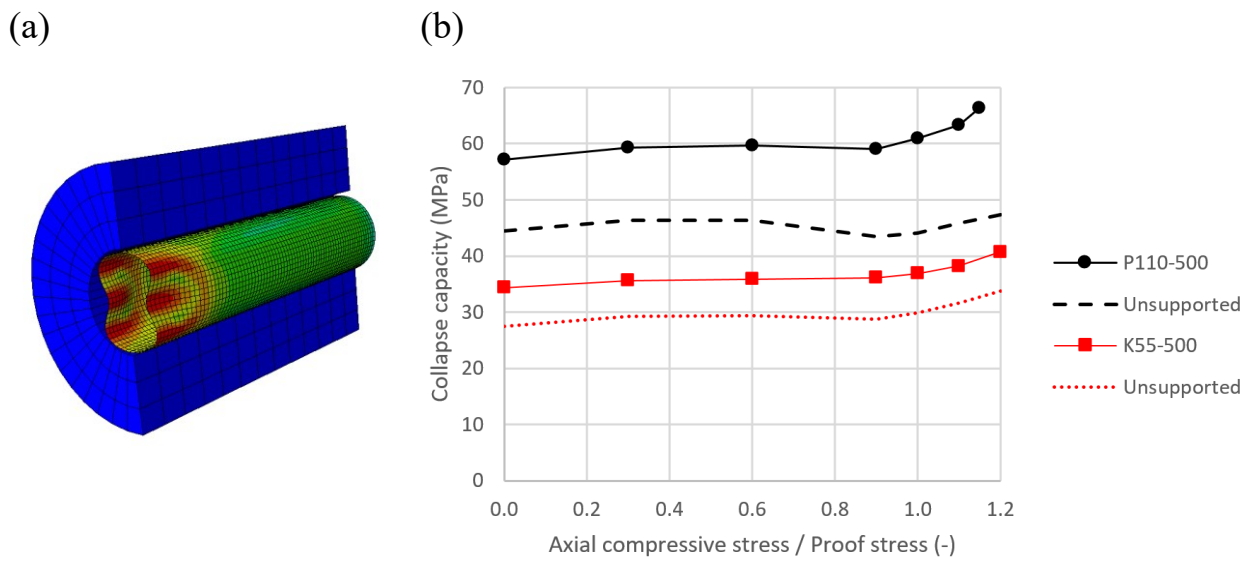

Figure 4: (a) Collapse deformation mode in supported condition (half the support is blanked out for visibility). (b) Predicted collapse capacity for K55 and P110 at 500 °C with supported and un-supported conditions.

3.4 Collapse capacity and OD/t ratio

In the following we will investigate the effect of OD/t ratio for the K55 and P110 materials. As in Section 3.3, we will focus on the materials at 500 °C. We could increase the diameter and the length and hold the thickness constant. However, for simplicity, and since the predicted collapse capacity will not alter, we chose to change the thickness to have three additional OD/t relations; 13.5, 23.1 and 27.8. The last OD/t relation correspond to a 13-3/8 in casing with a 12.2 mm wall thickness. Following the formulas in API TR 5C3, the selected OD/t ratios fully cover the 'plastic collapse' region and enters the neighboring 'yield strength collapse' and 'transition collapse' regions as shown in Figure 5. Thus, the most relevant OD/t ratios for plastic collapse is covered. Note that the borders of the different regions are defined from the yield strength of the materials and the OD/t ratios of the casing. Thus, regions are defined at different OD/t ratios for the K55 and the P110 materials.

The predicted collapse capacity from FEA is shown in Figure 6. Considering the K55 material, an increase in collapse capacity occurs for all selected OD/t ratios at high axial load. However, while the increase occurs at $0.9R_{p02}$ for the baseline OD/t=18.3, the increase starts at lower axial stress for the more thin-walled models (OD/t=23.1, 27.8), and higher axial stress for the thick-walled model (OD/t=13.5). The thin-walled models are prone to local axial buckling and could not reach higher axial stresses than the values shown in Figure 6 in the unsupported condition.

For the P110 material, the thin-walled models do not show significant sensitivity to the axial stress, while the thick-walled model (OD/t=13.5) enters a local minimum at $\sim 1.2R_{p02}$ before the collapse capacity increase (two additional FEA with $1.3R_{p02}$ and $1.4R_{p02}$ were performed). The collapse capacity as calculated from API TR 5C3 is also shown in Figure 6, and notably there is a strong correlation between FEA and the empirical API calculations for all OD/t ratios.

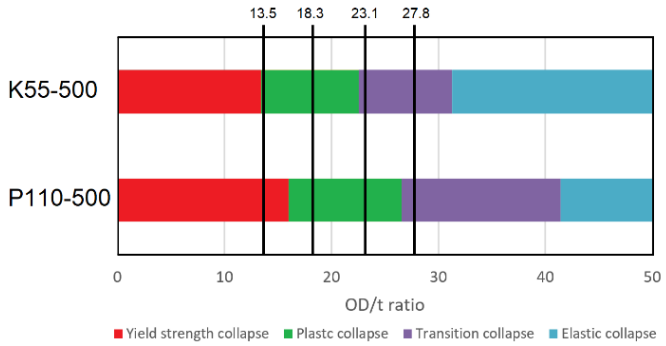

Figure 5: Range of the yield strength collapse, plastic collapse, transition collapse and elastic collapse regions for K55 and P110 at 500 °C following API TR 5C3

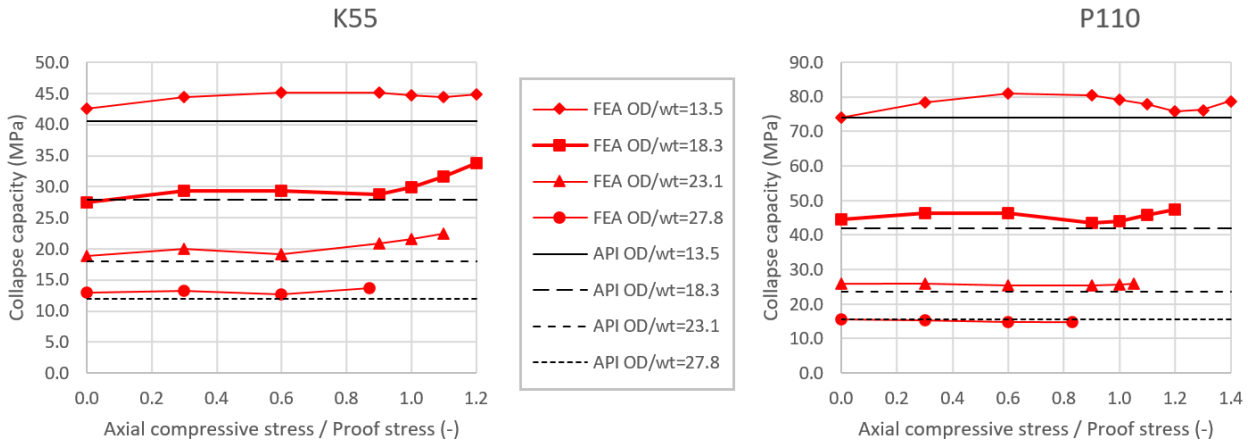

Figure 6: Predicted collapse pressure for various OD/t ratio for K55 and P110 at 500 °C. The predicted collapse pressure from API TR 5C3 is also shown

5. CONCLUSIONS

A numerical assessment of casings exposed to high axial compressive loads have been conducted. For axial compressive stresses above $\sim R_{p02}$, the collapse capacity increase for all 6 tested material/temperature combinations. When the casing is supported, the collapse capacity increases for all axial load conditions, and the distinct increase in collapse capacity occurs also here at the same axial load ($\sim R_{p02}$). For higher OD/t ratios, the increase in collapse capacity occurs at lower axial stress ($< R_{p02}$) and thin-walled casings are prone to local axial buckling. For lower OD/t ratios the increase in collapse capacity occurs at higher axial stress ($> R_{p02}$). It was found that the collapse pressure from FEA is high compared to the API TR 5C3 for room temperature and 350 °C material, while FEA and API TR 5C3 gives very similar capacity for materials at 500 °C. In this context it is noted that the FEA accounts for the significant reduction in the Young's modulus when increasing the temperature to 500 °C, while this effect is not accounted for by API TR 5C3. The main conclusion from the numerical study is that the collapse capacity increases when the casing is exposed to high axial compressive loading. However, it is noted that this is based on a model that simulates the conditions of a collapse pressure experiment and so does not account for all the complex phenomenon that can occur in a geothermal well. For instance could pressure loading from water pockets or thermal expansion in combination with cement-casing contact make an impact for the collapse capacity of an operational casing. Thus, more investigations are needed before firm conclusions can be made for practical design.

REFERENCES

American Petroleum Institute 2019. API Specification 5CT.

Buchmiller, D., Bjørset, A., Hørte, T. & Pettersen, S. Casing Collapse Design Using Structural Reliability Analysis for a Subsea Well on the Norwegian Continental Shelf. ASME 2018 37th International Conference on Ocean, Offshore and Arctic Engineering, 2018. V11BT12A030.

Dassault Systèmes, S. C. 2020. Abaqus version 2020 documentation.

Elders, W. A., Friðleifsson, G. Ó. & Albertsson, A. 2014. Drilling into magma and the implications of the Iceland Deep Drilling Project (IDDP) for high-temperature geothermal systems worldwide. *Geothermics,* 49**,** 111-118.

Friðleifsson, G. Ó., Elders, W. A. & Albertsson, A. 2014. The concept of the Iceland deep drilling project. *Geothermics,* 49**,** 2-8.

Gruben, G., Dillingh, B., Kaldal, G. S., Hoang, N.-H., Wollenweber, J., Rørvik, G., Thorbjornsson, I. & Nyhus, B. 2021. Thermo-mechanical tensile testing of geothermal casing materials. *Geothermics,* 89**,** 101944.

Hørte, T., Bjørset, A., Dan Tudor, Z. & Pettersen, S. Benefit From Structural Reliability Analysis in Risk Evaluation of Collapse of Externally Supported Casing. ASME 2020 39th International Conference on Ocean, Offshore and Arctic Engineering, 2020.

Kaldal, G. S., Jonsson, M. T., Palsson, H. & Karlsdottir, S. N. 2016. Structural modeling of the casings in the IDDP-1 well: Load history analysis. *Geothermics,* 62**,** 1-11.

New Zealand Standard 2015. NZS: 2403:2015 Code of practice for deep geothermal wells.